RSC Advances

PAPER

Cite this: *RSC Adv.*, 2020, **10**, 9878

Vacancy-induced interfacial ferromagnetic features in $SmFeO_3$-filled graphitic carbon foam†

Mahsa Fayazi,[a] Gao Shuai,[a] Bingyan Liu,[a] Li Lei,[b] Ivaturi Sameera,[c] Omololu Odunmbaku,[a] Shanling Wang,[d] Jiqiu Wen[d] and Filippo S. Boi *[a]

We report a novel structural and magnetic investigation of carbon foam (CFM) materials filled with $SmFeO_3$ crystals produced by (1) high temperature fusion between Sm_2O_3- and Fe_3C-filled carbon onions and (2) annealing of iron filled CFM with nanosized Sm_2O_3. Presence of a defect-rich monolayer-like CFM arrangement characterized by sharp interfaces with a $SmFeO_3$ single-crystal phase is demonstrated through TEM and HRTEM. Further, the presence of intense sp^3-rich features with variable carbonate content is evidenced by XPS and Raman spectroscopy. Complementary VSM, SQUID and ESR show also presence of intrinsic magnetization features which appeared to be attributable to the interfacial vacancy-rich regions of the graphitic CFM layers, as confirmed by Raman spectroscopy. Together with these signals, possible ferromagnetic contributions from the $SmFeO_3$ phase and α-Fe impurities are reported. These observations highlight therefore the presence of switchable interfacial magnetization features at the carbon/$SmFeO_3$ interface due to the variable concentrations of vacancies at the CFM interface, opening new directions towards applications in magnetic and interfacial-driven ferroelectric devices.

Received 24th December 2019
Accepted 1st March 2020

DOI: 10.1039/c9ra10854h

rsc.li/rsc-advances

Introduction

For many years, structural transformation phenomena involving the transition from graphite into diamond have been a subject of intense research and much interest in the fields of physics and materials science.[1–16] Early stage investigations of such transformations were reported by employing X-ray photoelectron spectroscopy (XPS) to demonstrate the presence of sp^3 to sp^2 transition during sequential annealing treatments under vacuum.[8] Particularly, the discovery of reversible transformations of nanosized diamonds into carbon nano-onions allowed for important breakthroughs into the dynamics of such structural transitions.[1–10] Reversible transformations were demonstrated by using laser-beam techniques with wavelengths of 532 nm and sample exposure times in the order of 20 min (for the nanosized diamond to carbon nano onion, CNO, transformation) and 40 min (for the reverted transformation into nano-diamond).[10]

High pressure studies applied to other systems such as peapods and solvated fullerenes have further demonstrated the possibility to trigger the formation of novel carbon-based materials with sp^3-rich characteristics and significant mechanical properties through a mechanism involving rehybridization of the chosen precursor-materials.[12,13] In addition to these important studies, recent reports have shown that creating direct interfaces between iron-based oxides and carbon materials can allow possible rehybridization effects with significant benefits not only for the control of sp^3-rich characteristics of the carbon layers but also for applications in electrical-memory devices.[14–18] In this context, rare-earth orthoferrites $RFeO_3$ (R = rare-earth ion) are a new class of materials with a distorted perovskite *Pbnm* structure which intrinsically exhibit canted ferromagnetism due to the presence of the 4f-electrons and 3d-electrons sublattices.[19] These materials have recently attracted significant attention for their important application perspectives in magnetic, ferroelectric and multiferroic devices. One of the most interesting features of these materials is the spin reorientation (SR). This property has been described as a magnetic phenomenon in which the easy axis of magnetization changes with another one under certain experimental conditions which are mostly related to the selected temperature and/or applied magnetic field.[18]

Interestingly, fabrication of monolayer carbon foam (MCFM)/$SmFeO_3$ interfaces has been recently demonstrated through a novel synthesis route involving high temperature fusion of Fe_3C filled CNOs with Sm_2O_3 filled CNOs and subsequent annealing.[17]

In fact, up to now, two main methodologies have been reported for the creation of CFM/orthoferrite interfaces, these consist into (1) high temperature fusion of as grown filled CNOs[17] and (2) annealing of as produced metal-filled carbon

[a]College of Physics, Sichuan University, Chengdu, China. E-mail: f.boi@scu.edu.cn
[b]Institute of Atomic and Molecular Physics, Chengdu, 610065, China
[c]Department of Physics, Guru Jambheshwar University of Science and Technology, Hisar, 125001, India
[d]Analytical and Testing Center, Sichuan University, Chengdu, 610064, China

† Electronic supplementary information (ESI) available. See DOI: 10.1039/c9ra10854h

foam materials with chosen oxides.[18] In those studies, the formation of a $SmFeO_3$ phase was investigated with major focus on the intrinsic magnetic properties of the orthoferrite. However, the structural and magnetic aspects of the residual graphitic carbon layers in direct interfacial contact with the orthoferrite phase were not investigated.[17]

Being interested in gaining a better understanding of the defect-richness properties and magnetic characteristic of the interfacial carbon layers in such CFM material, with particular emphasis in the samples produced with method 1, we have performed a novel structural and magnetic investigation by employing high resolution transmission electron microscopy (HRTEM), X-ray diffraction (XRD), X-ray photoelectron spectroscopy (XPS), Raman spectroscopy (RS), vibrating sample magnetometry (VSM), temperature dependent superconducting quantum interference device magnetometry (T-SQUID) and temperature dependent electron paramagnetic resonance (T-ESR).

Presence of a monolayer-like CFM arrangement with sharp interfaces with the $SmFeO_3$ single-crystal phase is demonstrated. XPS and RS revealed further presence of intense sp^3/vacancy-rich features with variable carbonate content. Particularly the defect components resulted to be more abundant in the samples produced with the method 1.

T-ESR evidenced presence of differential absorption features compatible with presence of interfacial vacancy-rich regions within the sample and therefore spontaneous defect-induced magnetic ordering below 300 K. In addition, magnetic contributions arising from encapsulated $SmFeO_3$ crystals and residual α-Fe could be detected by using VSM and SQUID magnetometry. The presented results imply presence of switchable interfacial magnetization features at the carbon/$SmFeO_3$ interface due to the existence of variable concentrations of defects in the CFM. Comparative analyses performed on vacancy-rich turbostratic and pyrolytic (doped/undoped) graphite samples further confirmed the above conclusion and underline the crucial role of vacancy defects towards creation of intrinsic magnetism in graphitic materials.[20–22]

Experimental

$SmFeO_3$ filled CFM hybrid structures were prepared following the fabrication method reported in ref. 17 and 18. Room temperature XRD measurements were performed with an Empyrean Panalytical diffractometer (Cu Kα1, Kα2). SQUID and VSM measurements of ZFC and FC curves were performed with Quantum Design systems from 300 K to 55 K (VSM) and from 300 K to 10 K (SQUID). TEM measurements were performed with a 200 kV American FEI Tecnai G2F20. T-ESR measurements were performed with a JEOL JES-FA200 at 300 K, 150 K and 77 K. XPS analyses were performed with an Escalab 250Xi, spot size of 500 micron. The Raman spectra were collected in a custom-built Raman system using a triple grating monochromator (Andor Shamrock SR-303i-B, EU) with an attached EMCCD (ANDOR Newton DU970P-UVB, EU), excitation by a solid-state laser at 532 nm (RGB lasersystem, NovaPro 300 mW, Germany) and collection by a 100× 0.90 NA objective (Olympus, Japan).

Results and discussion

The structural characteristics of the as annealed $SmFeO_3$ filled CFM samples were firstly revealed by TEM and HRTEM measurements, as shown in Fig. 1–3. These analyses evidenced presence of a single-crystalline-like arrangement in the encapsulated crystals, as shown in Fig. 1A by FFT (which shows an individual set of reciprocal lattice spots) and in Fig. 2 and 3.

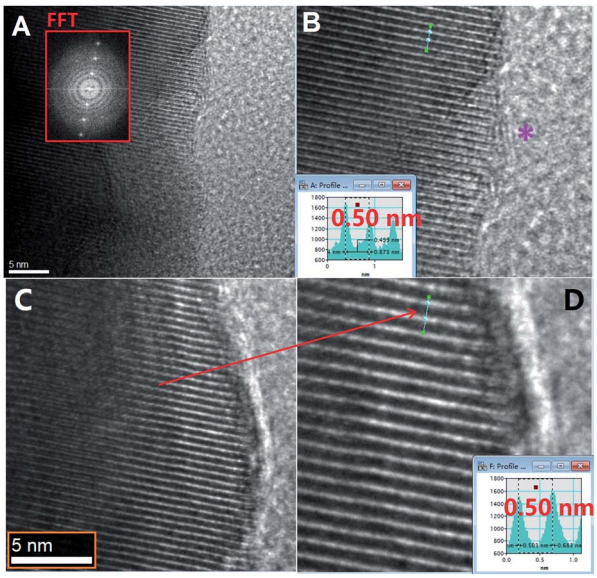

Fig. 1 HRTEM analyses of CFM type 1 revealing the presence of encapsulated $SmFeO_3$ single crystalline features (see FFT of crystal lattice in (A)-inset). In (C) and (D) the red arrow indicates a high detail of the $SmFeO_3$ lattice. In (B) the purple star indicates the presence of monolayer-like carbon features with a defective (vacancy-rich) arrangement.

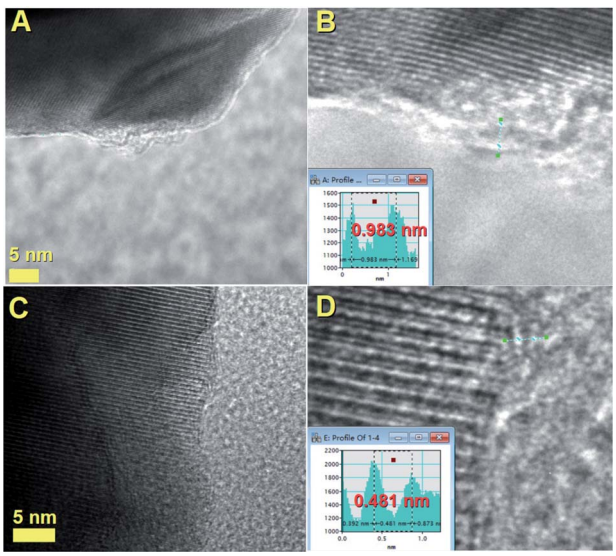

Fig. 2 HRTEM analyses of CFM type 1 revealing the presence of encapsulated $SmFeO_3$ single crystalline features in additional areas. The high detail of the $SmFeO_3$/C interface in D and profile analyses indicate the presence of vacancy-like defects in the carbon layers.

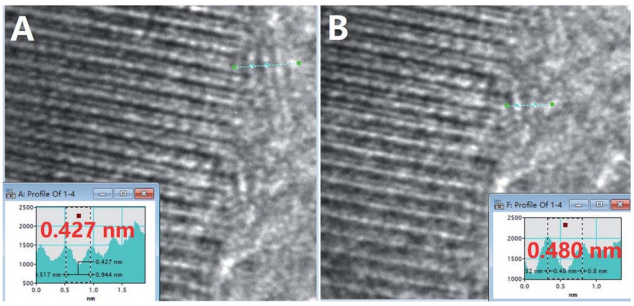

Fig. 3 HRTEM analyses (A and B) of CFM type 1 revealing the presence of vacancies in different regions of the carbon layers. Presence of these defect features can be considered the origin of the observed ferromagnetic components in the ESR spectra.

Existence of variable monolayer-like features with a defect rich arrangement was also found, as indicated by the purple star in Fig. 1B and the profile analyses in Fig. 3A and B. Presence of $SmFeO_3$ crystal-phases with space group *Pbnm* within the CFM was further confirmed by XRD analyses, as shown in Fig. 4. Investigation of the sp^3/sp^2 characteristics of the CFM graphitic carbon layers was then sought by XPS. As shown in Fig. 5, measurements performed in CFM samples produced with method-1 (Fig. 5A) and method-2 (Fig. 5B) revealed the presence of sp^3-rich characteristics together with a variable level of carbonate (C–O rich) content. Interestingly, the level of C–O content was found to decrease especially in the CFM produced

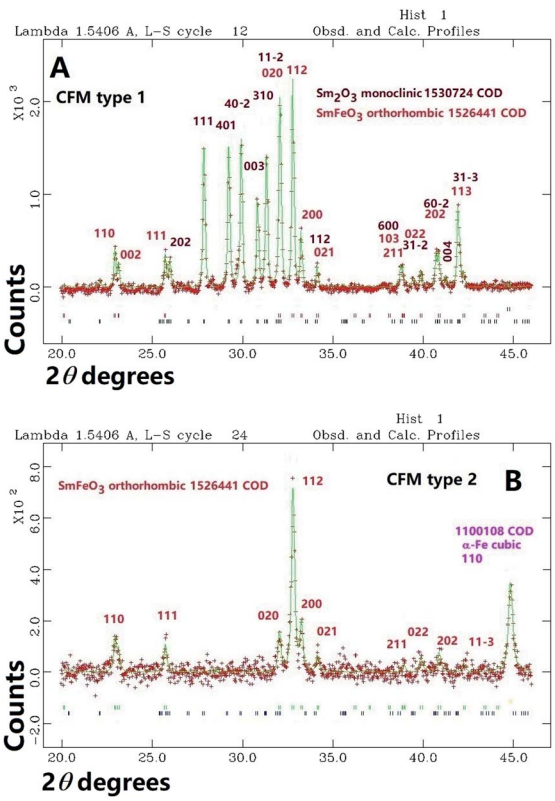

Fig. 4 XRD measurements (red crosses) and Rietveld refinement analyses (green line) of CFM type 1 and 2 revealing the presence of lattice reflections compatible with $SmFeO_3$.

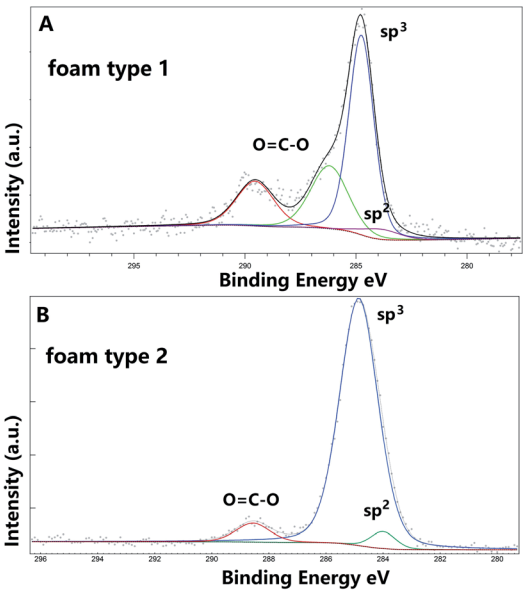

Fig. 5 XPS analyses showing the presence of sp^3-rich features in both CFM type 1 and CFM type 2 ((A) and (B) respectively).

with method-2, implying possible variation in the carbon layer defect-concentration. Both the XPS samples analyses shown in Fig. 5A and B for CFM type 1 and 2 respectively revealed a high sp^3-rich content possibly resulting from the annealing stage.[15] However, the larger C–O content observed in the type 1 CFM may be attributable to a higher quantity of structural defects in the produced CFM.

Further investigations were then sought by Raman spectroscopy experiments. As shown in ESI Fig. 1† Raman

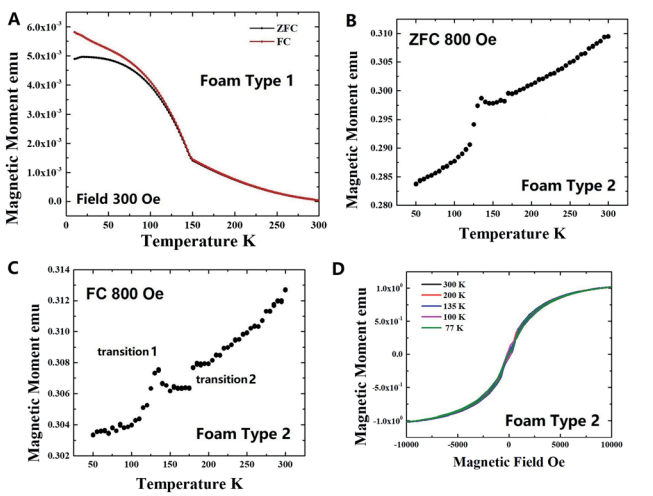

Fig. 6 Magnetization analyses of CFM type 1 (A) and CFM type 2 (B–D) revealing the presence of a significant magnetic transition in both the type of samples at approximately 150 K. In D the large values of the measured saturation magnetization are attributable to the presence of residual α-Fe within the CFM type 2 sample.The transition 1 at about 140 K in CFM type-1 sample appears to be due to Fe_3O_4 (high ferrimagnetic phase) with Verwey transition expected in a wide temperature range 120–140 K.[29,30] However, XRD measurements do not support the presence of such iron oxide phase in the present samples.

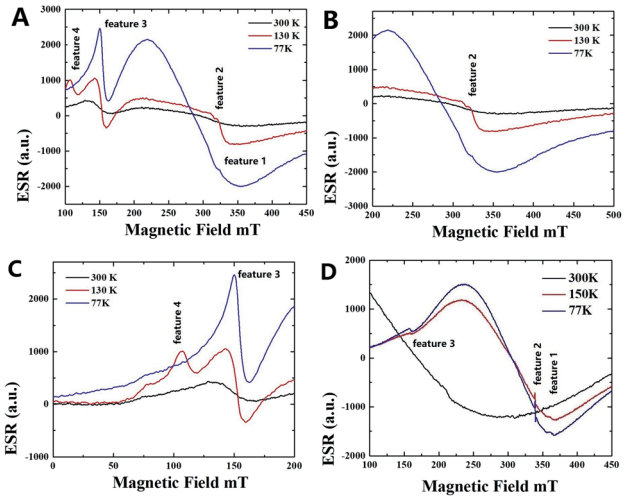

Fig. 7 ESR spectra acquired from different portions of the CFM powder (portion 1 in A–C and portion 2 in D of the same powdered sample). Note the presence of 4 peak features which may be attributable to (1) $SmFeO_3$ magnetic moments (feature 1), (2) π-electrons of the CFM, (3) defect induced ferromagnetic-components and (4) antiferromagnetic transition occurring in some portion of the encapsulated $SmFeO_3$ phase due to enhanced contribution of Sm magnetic moments. Note that no additional iron oxide phases were detected in the XRD and Rietveld refinement analyses.[29,30]

spectroscopy analyses of CFM type 1 revealed presence of significantly intense D band features and absence of G band in agreement with the XPS analyses in Fig. 5. Further analyses were then performed by using magnetometry and ESR spectroscopy, in an attempt to estimate the nature of the components involved in the magnetization signals within CFM samples. As shown in Fig. 6A, ZFC and FC measurements of CFM type 1 revealed the presence of a gradual increase in the magnetization with the decrease of the temperature, together with a significant transition at the temperature of 150 K. Interestingly a similar transition could be probed in the CFM type 2 (Fig. 6B and C), with a magnetization peak at approximately 150 K, which could be ascribed to a transition in the magnetic structure of the $SmFeO_3$ phase induced by the Sm magnetic moments (antiferromagnetic exchange interaction between the two magnetic sublattices).[17,18] On the basis of the XRD measurements in Fig. 4, no contribution was detected from other iron oxide phases. In addition, magnetization *vs.* field analyses revealed presence of another magnetic component attributable to the residual α-Fe phase within the CFM sample.[18]

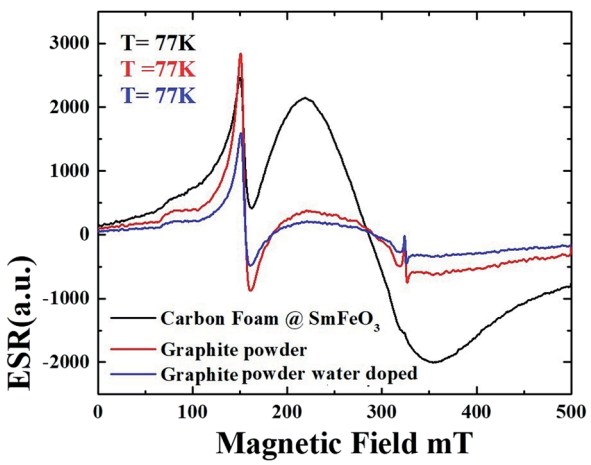

Fig. 8 ESR spectra at 77 K acquired from CFM type 1, turbostratic graphite powder and water doped turbostratic graphite powder. A significant overlap in the defect-induced ferromagnetic feature is observable in all the three samples, allowing to conclude the presence of vacancy induced ferromagnetism in the CFM type 1 in analogy with the graphite samples.

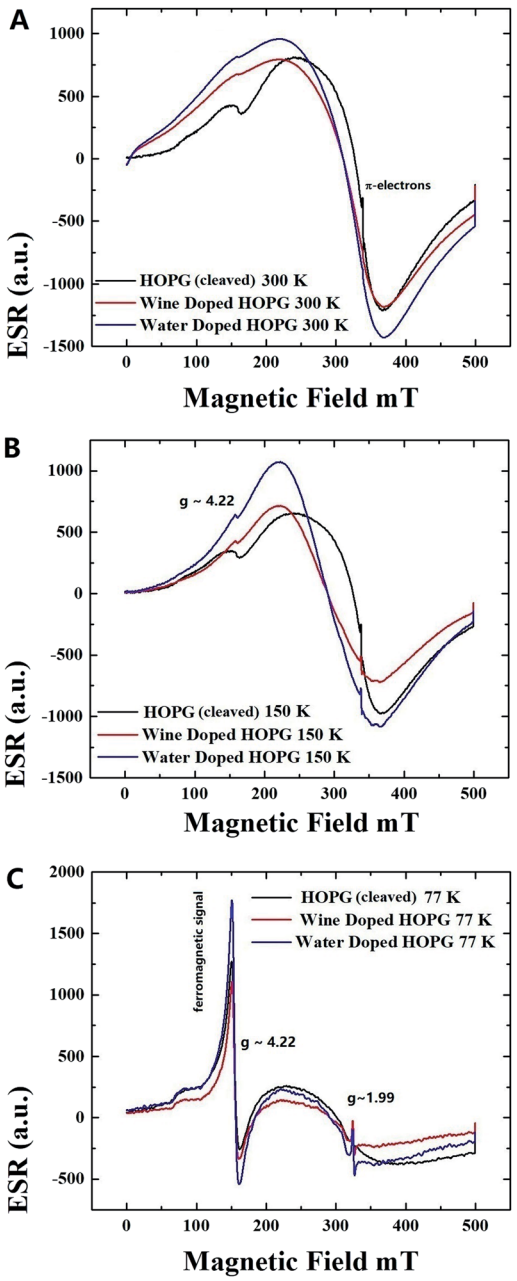

Fig. 9 ESR measurements of vacancy-rich HOPG flakes: undoped (black), wine doped (red) and water doped (blue). Note the presence of a dominant differential absorption feature for *g*-values of ~4.22 attributable to vacancy induced ferromagnetism.

Further insights on the overall components involved in the magnetization process were then sought by ESR analyses of the CFM produced with the method 1. As shown in Fig. 7A–C, measurements performed in different portions of the CFM powder (Fig. 7A and D) revealed a temperature-dependent signal characterized by π-electron related features (feature 2 in Fig. 7A–D) with variable intensities and possible ferromagnetic components (feature 3) which appeared to enhance in intensity as the temperature decreased from 300 K to 77 K. In addition to these observations, another feature (feature 4) possibly representing the magnetic transition observed in Fig. 6 was found at 150 K. The presence of a variable intensity of the feature 3 in Fig. 7A–D can be possibly ascribed to local variation in the concentration of magnetism-related defects in the interfacial regions of the CFM sample. In the attempt to further confirm this interpretation, the CFM signal measured at 77 K was further compared to those measured in graphite and water-treated graphite samples which have been reported to contain ferromagnetic components in recent reports.[20–22] As shown in Fig. 8 it seems clear that the obtained signal from graphite powder and water doped graphite powder significantly overlaps with that of the CFM measured in this work. This observation unambiguously confirms the presence of defect-induced ferromagnetic features in the produced CFM sample.

In an attempt to further verify the origin of the aforementioned intrinsic magnetic signals, additional comparative ESR measurements were then performed in highly oriented pyrolytic graphite samples (HOPG) characterized by vacancy-like defect-rich features as shown in Fig. 9.[23,24] Typical ESR measurements obtained in HOPG flakes before and after doping through intercalation methods (see ref. for the used intercalation methods based on water and wine doping[26–28]) revealed a similar trend, with the appearance of a common differential absorption features compatible with vacancy induced ferromagnetism for g values of $\sim$4.22 at temperatures below 200 K (it is important to notice that the vacancy signals resulted approximately unmodified by the doping method).

Conclusion

In conclusion we have reported a novel investigation on the magnetic properties of $SmFeO_3$ filled CFM materials. Presence of a vacancy-rich CFM arrangement with sharp $SmFeO_3$/C monolayer-like interfaces was revealed, as demonstrated by XPS and Raman spectroscopy analyses. ESR particularly revealed presence of multiple magnetization features which appeared to be attributable to (1) the interfacial vacancy-rich regions of the CFM layers (2) the canted ferromagnetism of the $SmFeO_3$ phase. These findings were further supported by comparative T-ESR and SQUID measurements performed on vacancy rich undoped and doped pyrolytic graphite samples.

Conflicts of interest

There are no conflicts of interest to declare.

Acknowledgements

We acknowledge the Sichuan Province Technology Grant No. 2019YFH0080. We also acknowledge professor Anna Corrias for the help in checking the manuscript.

Notes and references

1 R. S. Lewis, T. Ming, J. F. Wacker, E. Anders and E. Steel, Interstellar diamonds in meteorites, *Nature*, 1987, **326**, 160–162.
2 O. Guillois, G. Ledoux and C. Reynaud, Diamond Infrared Emission Bands in Circumstellar Media, *Astrophys. J.*, 1999, **521**, L133–L136.
3 M. Goto, T. Henning, A. Kouchi, H. Takami, Y. Hayano, T. Usuda and A. C. Andersen, Spatially resolved 3 μm spectroscopy of Elias 1: Origin of Diamonds in Protoplanetary Disks, *Astrophys. J.*, 2009, **693**, 610–616.
4 D. Ugarte, Curling and closure of graphitic networks under electron beam irradiation, *Nature*, 1992, **359**, 707–709.
5 M. Chhowalla, H. Wang, N. Sano, K. B. K. Teo, S. B. Lee and G. A. Amaratunga, J. (interstellar) Carbon Onions: Carriers of the 217.5 nm Interstellar Absorption Feature, *Phys. Rev. Lett.*, 2003, **90**, 155504.
6 L. Hultman, S. Stafstrom, Z. Czigany, J. Neidhardt, N. Hellgren, I. F. Brunell, K. Suenaga and C. Colliex, Cross-Linked Nano-onions of Carbon Nitride in the Solid Phase: Existence of a Novel $C_{48}N_{12}$ Aza-Fullerene, *Phys. Rev. Lett.*, 2001, **87**, 225503.
7 F. Banhart, E. Hernandez and M. Terrones, Extreme Superheating and Supercooling of Encapsulated Metals in Fullerene like Shells, *Phys. Rev. Lett.*, 2003, **90**, 185502.
8 T. Petit, J.-C. Arnault, H. A. Girard, M. Sennour and P. Bergonzo, Early stages of surface graphitization on nanodiamond probed by X-ray photoelectron spectroscopy, *Phys. Rev. B*, 2011, **84**, 233407.
9 A. M. Panich, A. I. Shames, N. A. Sergeev, M. Olszewski, J. K. McDonough, V. N. Mochalin and Y. Gogotsi, Nanodiamond graphitization: a magnetic resonance study, *J. Phys.: Condens. Matter*, 2013, **25**, 245303.
10 J. Xiao, G. Ouyang, P. Liu, C. X. Wang and G. W. Yang, Reversible Nanodiamond-Carbon Onion Phase Transformations, *Nano Lett.*, 2014, **14**, 3645–3652.
11 J. Xiao, P. Liu, L. Li and G. Yang, Fluorescence origin of nanodiamonds, *J. Phys. Chem. C*, 2015, **119**, 2239–2248.
12 W. Cui, M. Yao, S. Liu, F. Ma, Q. Li, R. Liu, B. Liu, B. Zou, T. Cui and B. Liu, A New Carbon Phase Constructed by Long-Range Ordered Carbon Clusters from Compressing C70 Solvates, *Adv. Mater.*, 2014, **26**, 7257–7263.
13 X. Yang, M. Yao, X. Wu, S. Liu, S. Chen, K. Yang, R. Liu, T. Cui, B. Sundqvist and B. Liu, Novel Superhard sp^3 Carbon Allotrope from Cold-Compressed C70 Peapods, *Phys. Rev. Lett.*, 2017, **118**, 245701.
14 X. Zhang, S. Wang, Y. He and F. S. Boi, Mapping the transition from carbon-onions filled with Fe_3C to carbon-foam completely filled with α-Fe: unlocking mass-

production of ferromagnetic carbon foam, *Mater. Today Commun.*, 2018, **14**, 72–76.
15 F. S. Boi, X. Zhang and D. Medranda, Evidence of sp^3-rich nano-diamond-like characteristics in amorphous carbon foam continuously filled with α-Fe, *Diamond Relat. Mater.*, 2018, **84**, 190–195.
16 X. Zhang, D. Medranda, O. Odunmbaku, A. Taallah and F. S. Boi, Wustite-induced formation of sp^3-rich faceted carbon foam: the key role of cooling rate on sp^3-abundance (and oxide crystal-habit) control, *Mater. Today Commun.*, 2018, **16**, 250–257.
17 F. S. Boi, X. Zhang, D. Medranda, O. Odunmbaku, A. Taallah and S. Wang, Fabrication of graphene-oxide/$SmFeO_3$ interfaces by ambient pressure/high-temperature fusion of Fe_3C@CNOs with Sm_2O_3@C-capsules, *Mater. Today Commun.*, 2019, **18**, 81–86.
18 J. Wang, S. Ivaturi, S. Wang, A. Corrias and F. S. Boi, Observation of enhanced magnetic transition in Pbnm $SmFeO_3$, *J. Appl. Phys.*, 2017, **122**, 174103.
19 G. Volonakis and F. Giustino, Ferroelectric Graphene–Perovskite Interfaces, *J. Phys. Chem. Lett.*, 2015, **6**, 2496–2502.
20 X. Yang, H. Xia, X. Qin, W. Li, Y. Dai, X. Liu, M. Zhao, Y. Xia, S. Yan and B. Wang, Correlation between the vacancy defects and ferromagnetism in graphite, *Carbon*, 2009, **47**, 1399–1406.
21 X. Miao, S. Tongay and A. F. Hebard, Extinction of ferromagnetism in highly ordered pyrolytic graphite by annealing, *Carbon*, 2012, **50**, 1614–1618.
22 Z. He, H. Xia, X. Zhou, X. Yang, Y. Song and T. Wang, Raman study of correlation between defects and ferromagnetism in graphite, *J. Phys. D: Appl. Phys.*, 2011, **44**, 085001.
23 A. Eckmann, A. Felten, A. Mishchenko, L. Britnell, R. Krupke, K. S. Novoselov and C. Casiraghi, Probing the Nature of Defects in Graphene by Raman Spectroscopy, *Nano Lett.*, 2012, **12**, 3925–3930.
24 R. N. Bhowmik, Ferromagnetism in lead graphite-pencils and magnetic composite with $CoFe_2O_4$ particles, *Composites, Part B*, 2012, **43**, 503–509.
26 K. Deguchi, Y. Mizuguchi, Y. Kawasaki, T. Ozaki, S. Tsuda, T. Yamaguchi and Y. Takano, Alcoholic beverages induce superconductivity in $FeTe_{1-x}S_x$, *Supercond. Sci. Technol.*, 2011, **24**, 055008.
27 K. Deguchi, T. Okuda, H. Hara, S. Demura, T. Watanabe, H. Okazaki, M. Fujioka, S. J. Denholme, T. Ozaki, T. Yamaguchi, H. Takeya, F. Saito, M. Hisamoto and Y. Takano, Tartaric acid in red wine as one of the key factors to induce superconductivity in $FeTe_{0.8}S_{0.2}$, *Physica C*, 2013, **487**, 16–18.
28 T. Scheike, W. Böhlmann, P. Esquinazi, J. Barzola-Quiquia, A. Ballestar and A. Setzer, Can Doping Graphite Trigger Room Temperature Superconductivity? Evidence for Granular High-Temperature Superconductivity in Water-Treated Graphite Powder, *Adv. Mater.*, 2012, **24**, 5826.
29 R. N. Bhowmik, S. Kazhugasalamoorthy and A. K. Sinha, Role of initial heat treatment of the ferrite component on magnetic properties in the composite of ferrimagnetic $Co_{1.75}Fe_{1.25}O_4$ ferrite and non-magnetic $BaTiO_3$ oxide, *J. Magn. Magn. Mater.*, 2017, **444**, 451–466.
30 R. N. Bhowmik, P. Mitra, R. J. Choudhury and V. R. Reddy, Substrate effect on the structural phase formation and magnetic properties of α-Fe_2O_3 and Ti doped α-Fe_2O_3 thin films, *Appl. Surf. Sci.*, 2020, **501**, 144224.